Chapter 4

Green synthesis of reduced graphene oxide using *Tinospora cordifolia* plant extract: Exploring its potential for methylene blue dye degradation and antibacterial activity

Abstract

Graphene has attracted significant attention recently due to its unique mechanical, electrical, thermal, and optical properties. The present study focuses on synthesizing green rGO using *Tinospora cordifolia* plant stem extract by mixing it in a suspension of graphene oxide. The plant extract of *T. cordifolia* acts as a reducing agent and is cost-effective, renewable, and eco-friendly. Green synthesized rGO (G-rGO) was characterized using FTIR, HR-SEM, EDX, and HR-XRD analysis. G-rGO consists of nanosheets with an average width of approximately 30 nm. G-rGO has a range of hydrodynamic radius (270-470) nm and an average zeta potential of -29.9 mV. Further, G-rGO was used as a nano-adsorbent for optimal exclusion of Methylene Blue (MB) dye using Response surface methodology (RSM). Adsorption results confirmed 94.85% MB dye removal with 58.81 mg/g adsorption capacity at optimum conditions. The G-rGO's antibacterial activity was also tested against *Staphylococcus aureus* (gram-positive) and *Escherichia coli* (gram-negative) bacteria and found the exhibited zone of inhibition 10, 11, and 15 mm and 10, 13, 17 mm at 20, 40, and 80 µg/mL concentrations of G-rGO, respectively.

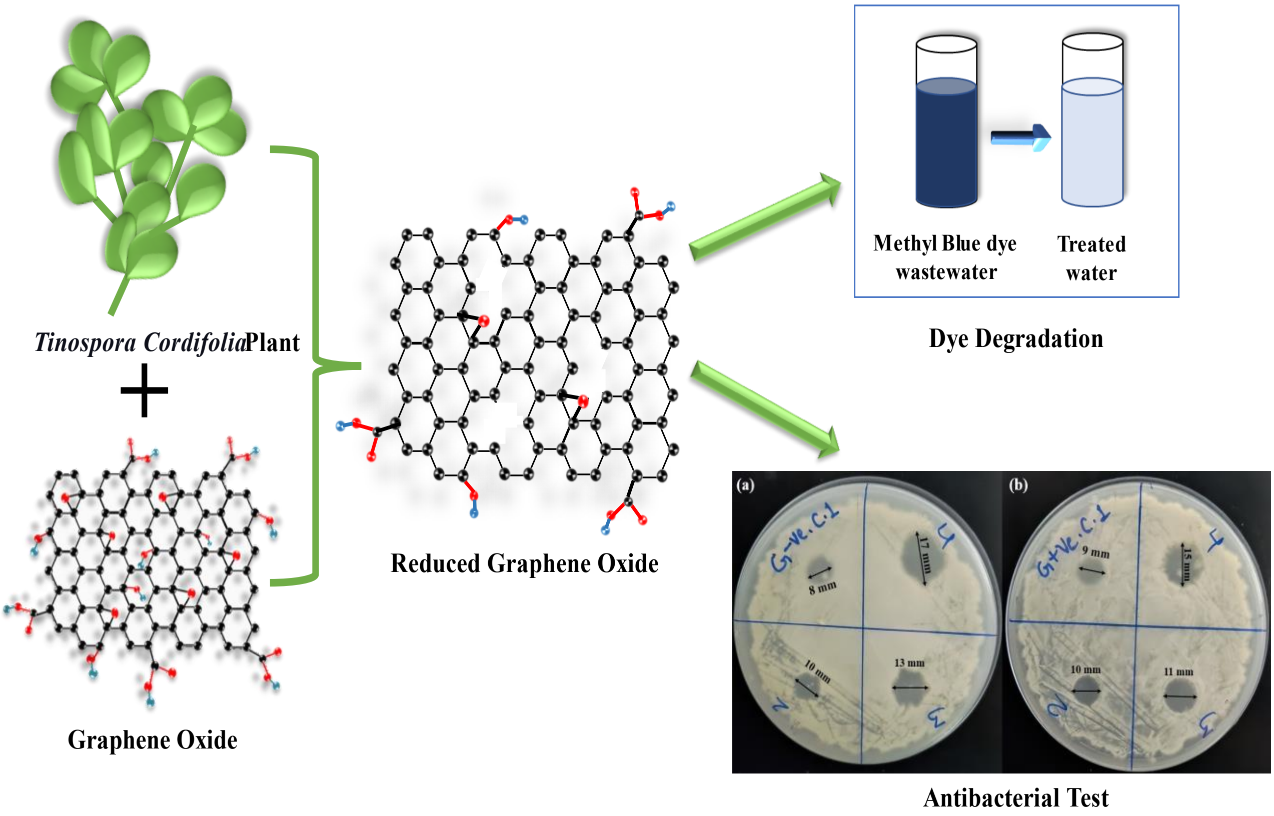
Tinospora Cordifolia Plant
+
Graphene Oxide
Reduced Graphene Oxide
Methyl Blue dye wastewater
Treated water
Dye Degradation
(a)
G-ve.C.1
8 mm
17 mm
10 mm
13 mm
(b)
G+ve.C.1
9 mm
15 mm
10 mm
11 mm
Antibacterial Test

4.1. Introduction

Heterocyclic organic dyes are used in the cosmetic, culinary, plastic, leather, textile, paper, and pharmaceutical sectors. Methylene blue (MB) is also a heterocyclic dye and is the most commonly used dye [129,130]. However, these sectors released an enormous volume of effluent into the surrounding environment that could have severe carcinogenic consequences, including *nausea, vomiting, diarrhea,* the development of the *Heinz bodies, jaundice, cyanosis, tissue necrosi*s, *quadriplegia,* disruption of the environment, and disturbances in the aquatic biodiversity. This calls for the complete and effective removal of MB dye [130,131]. Consequently, a variety of techniques have been used to reduce carcinogenic dyes that were earlier discussed in Chapter 1. Therefore, developing an adsorbent-based solution that is affordable, easy to recover from, and highly efficient in the degradation of MB dye is imperative. Owing to its many active sites, excellent electron transfer capacity, high surface-to-volume ratio, high Fermi potential, superior manipulation, and high levels of thermal, chemical, and physical stability.

Nanoparticles (NPs) have recently captured the interest of the dye degradation field [132]. Several nanoparticles, including Au, Ag, Pd, and Pt, have been widely used to accelerate the degradation of dye materials [130]. The above-mentioned precious metal nanoparticles have several drawbacks, such as expensive cost, limited supply, and production of negative effects like eye discomfort, *argyria* (blue or blackish pigmentation), and skin allergy, which waned the desire for these valuable metal nanoparticles. Therefore, much attention has been paid to Fe, Cu, Ni, and Co (non-precious metal nanoparticles) to use as catalysts for the degradation of MB dye [130]. The emphasis on Fe_3O_4 nanoparticles among non-precious metal oxide nanoparticles is appealing because of their reactive surfaces, low cost, high specific area, faster magnetic separation after decomposition, reduced environmental pollution, and quickly oxidized surface [133,134]. Fe_3O_4 nanoparticles quickly lose their active sites when reacting with organic dye, causing a high-speed nanoparticle agglomeration that cannot entirely break down the substance of the dye. The restrictions mentioned above might be overcome if the Fe_3O_4 NPs were adequately supported by active carbon. Graphene, carbon nanotubes, Vulcan carbon, and other carbonaceous nanomaterials are frequently used as supports to bind nanoparticles [130]. The high electron transfer rate, tremendous surface area, better mechanical, electrical, charge carrier mobility, elastic behavior, and chemical and thermal characteristics of graphene make it much superior to the other carbon supports listed above [31]. With a high surface area and exceptional adsorption capabilities, graphene-based materials efficiently remove pollutants such as heavy metals, organic compounds, and dyes from water and air, contributing to environmental cleanup efforts. Moreover, their strong antibacterial properties make them effective agents against a wide range of pathogenic bacteria, offering potential solutions for combating bacterial infections and promoting public health. Chemical vapor deposition (CVD), solution-based chemical reduction, mechanical and ultrasonic exfoliation, epitaxial growth, electric arc discharge, and others are currently used to produce graphene on a large scale [33,130,135,136]. These techniques have several limitations, such as the need for high temperatures and complex equipment, the production of lesser yields, labor, time, and money-intensive characteristics. Because of this, a different approach based on the reduction of graphene oxide (GO) has been developed, and the resulting reduced graphene oxide (rGO) demonstrated higher conductivity (0.05 and 2 S cm^{-1}), which is roughly three times higher magnitude than the GO and also comparable to graphene. Restoring a graphitic network of sp^2 bonds is responsible for the increased surface area, effective carrier mobility, and improved electro-catalytic characteristics of rGO over GO [137,138]. Primarily, powerful reducing chemicals such as di-methyl hydrazine [31], hydroquinone [32], and hydrazine hydrate [33] are used to reduce GO. However, those above potent reducing agents showed some drawbacks, including the bonding of toxic elements and atoms of elemental nitrogen, the generation of toxic gases, and the partial elimination of oxygen-containing species, which endanger the environment and lower the effectiveness of rGO. Tin powder [139] and iodide [140] have additionally been utilized as efficient reducing agents for the total reduction of GO in addition to those mentioned above traditional reducing agents. The rGO possesses carboxyl groups (-COOH), carbonyl groups (C=O), hydroxyl groups (-OH), and epoxide groups (-O-), providing a diverse range of active sites for the adsorption of hydrophobic water pollutants. Tin substances have negative side effects, including thyroid gland tumours, genotoxicity, neurotoxicity, cutaneous toxicity, immunotoxicity, and hepatotoxicity. On the other hand, Iodideas can potentially have serious negative consequences on the human body, including hand numbness, pulmonary oedema, *hyperthyroidism arrhythmia*, and heart failure [130]. The major goal of the dye removal strategy is to reduce the degree of environmental toxicity, which cannot be achieved if those above powerful reducing agents enhance the toxicity of rGO sheets. Due to its eco-friendly methods, time and cost-efficient features, the tendency for highly developed and intricate equipment, etc., renewable materials, particularly photosynthetic autotrophs mediated GO reduction, have attracted curiosity. Photosynthetic autotrophs can reduce metal ions in addition to GO sheets.

The present study focuses on the sustainable synthesis of rGO using *T. cordifolia* stem extracts and application in removing MB. The response surface methodology (RSM) was used to analyze varied parameters like initial dye concentration, pH, catalyst dose, and adsorption time of the adsorption process. The effect of G-rGO's antibacterial activity was also elucidated. Further, *Staphylococcus aureus* (gram-positive) and *Escherichia coli* (gram-negative) bacteria were used to investigate the bactericidal efficacy of bacterial pathogens. The feeds were characterized using XRD, FTIR, SEM, zeta potential, particle size analyzer, and UV-vis spectrometer.

4.2. Materials and Methodology

4.2.1 Materials

Pristine graphite powder (99% carbon, 325 mesh) and Methylene Blue dye were ordered from Sigma Aldrich, India. All the chemicals were used without treatment or purification in the experimental study and were analytical grade.

4.2.2 Extract preparation of T. cordifolia plant stem

T. cordifolia plant stems were collected and washed with distilled water several times and then chopped and crushed. Further, 15 g washed *T. cordifolia* stems were added in a 250 mL flask with 100 mL distilled water and boiled for 3 h with constant stirring at 80-90°C [141,142]. The solution's hue changed from colorless to brown and cooled until it reached room temperature. The prepared solution was filtered using Whatman filter paper (No.1). The sample was collected in a glass vial and stored in the refrigerator at (0-5°C) for one week.

4.2.3 Preparation of GO

GO was synthesized from natural graphite powder using modest tweaks to Hummer's process (**Fig. 4.1a**). 5.0 g of dried graphite powder and 0.015 g of boric acid (H_3BO_3) were added to 120 mL of concentrated sulfuric acid (0.1M H_2SO_4) in a 1000 mL flask held in an ice bath (0-5°C). The solution was constantly stirred for roughly 3 h [143]. The combination was placed in an ice bath (<15°C to avoid explosion) for 2 h and slowly added 15 g of $KMnO_4$. The solution was to be removed from the ice bath and start heating to 35°C for 2 h, stirring constantly. The stirred mixture was diluted with 450 mL of deionized water and heated to 95°C for 2 h. Thereafter, the mixture was allowed to settle to an ambient temperature for 1 h. Furthermore, 35 mL of hydrogen peroxide (H_2O_2, 30 %) was added to eliminate $KMnO_4$ residue. Finally, the solution was filtered (Whatman No. 1 filter paper, vacuum filtration), and the resulting precipitate was thoroughly rinsed with 500 mL of deionized water and dried in a hot air oven for 15 h at 85°C.

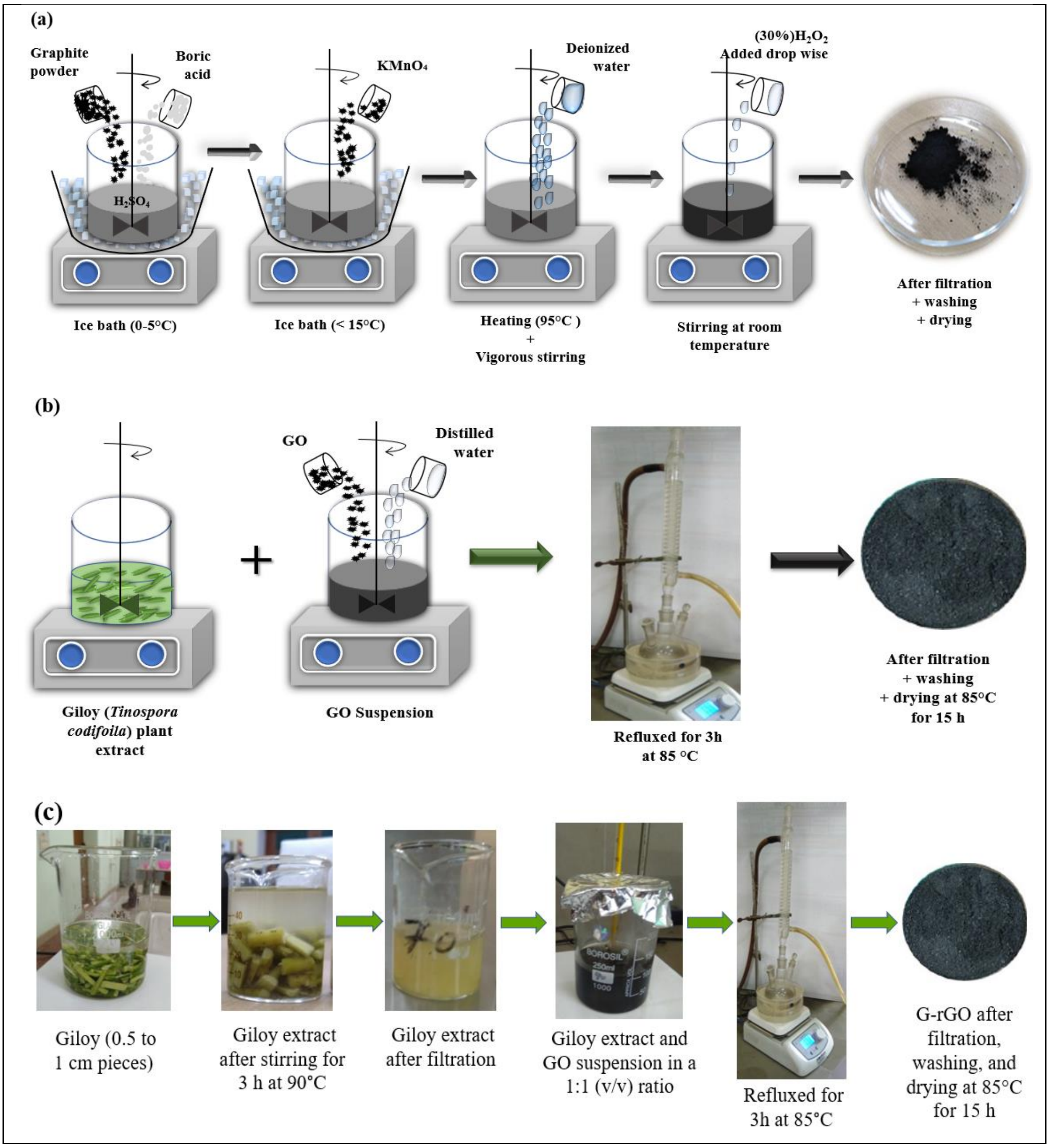

Fig. 4. 1 (a) A schematic illustration of the GO's using modified Hummer's method, (b) An illustration of the G-rGO from *T. cordifolia*, and (c) A typical presentation of green synthesis of G-rGO from *T. cordifolia* plant extract.

4.2.4 Green synthesis of rGO using T. cordifolia stem extract

A 50 mL solution of distilled water containing 25 mg of GO was sonicated for 1 h in a 100 mL Erlenmeyer flask. Further, an Erlenmeyer flask (250 mL) was used to combine 50 mL T.

cordifolia extract and 50 mL GO suspension in a 1:1 (v/v) ratio. The thoroughly mixed solution was refluxed at 85°C for 3 h [142]. Finally, the resulting solution was filtered (Whatman filter paper (No.1)), rinsed multiple times, and dried in the oven (85°C) for 15 h. The dried G-rGO was ground into a fine powder for further experiments (Fig. 4.1b).

4.2.5 Characterization of GO and G-rGO

The structural characteristics of GO and G-rGO were identified using the Rigaku SmartLab 9kW Powder X-ray diffraction system with Cu-Kα radiation source (30 kV, 30 mA) keeping $\lambda = 1.5406$ nm. The range of 2θ was 10–80° used to obtain the diffraction patterns with a 5° per minute scan rate. Further, SEM-EDX (MA15/18, Carl Zeiss Microscopy equipped with Team Pegasus Integrated EDS-EBSD with octane plus and Hikari Pro) was used to display the images of the surface and elemental percentage of GO and G-rGO. A Malvern Panalytical, Zetasizer Ver. 7.13 zeta potential analyzer was used to analyze the distribution of hydrodynamic particle size of GO and G-rGO and their zeta potential stability in colloidal solutions. The solution was prepared in 50 mL of distilled water by mixing 1 mg of GO and G-rGO powder, respectively. FT-IR technique (Nicolet iS5, THERMO Electron Scientific Instruments LLC) was used to estimate the surface functional groups of GO, G-rGO, and *T. cordifolia* plant extract. FTIR spectrophotometer was employed to obtain the spectra, which have spectral resolutions of 4 cm^{-1} step size of 1 s, and an infrared wavelength range of 4000-500 cm^{-1}. The absorbance of the aqueous MB dye solution at the λ_{max} (664 nm) was measured in a UV-vis spectrophotometer (SL-159, Elico, India) using a quartz cuvette to determine the sample concentration in the aqueous GO and G-rGO solution.

4.2.6 Batch adsorption experiments

MB dye was removed by batch adsorption using G-rGO. One Erlenmeyer flask (250 mL) containing MB dye solutions (100 mL) was used for adsorption experiments. To maximize the MB dye's adsorption, the effects of several variables were examined, including the initial pH of the solution, initial dye concentration, and duration of adsorption. Drop-by-drop additions of 0.1M HCl and 0.1M NaOH solution were used to change the solution's initial pH. An incubator shaker (REMI, India) with temperature control was used to perform adsorption experiments. The range of temperature fluctuations in the incubator was 30±5°C and 130 rpm agitation speed. The following equations (1 and 2) were employed to estimate the % removal of the MB dye and the adsorption capacity of the adsorbent [144].

$$\% R = \frac{(C_0 - C_t)}{C_0} \times 100 \tag{1}$$

$$q_t = \frac{(C_0 - C_t)}{w} \times V \tag{2}$$

Where C_0 and C_t represent the initial concentration and concentration at any time t of the MB dye solution (mg/L) respectively, V is the volume of the dye solution, w represents the amount of adsorbent (g), % R represents the percentage removal of MB, and q_t represents the adsorption capacity of the adsorbent (mg/g). The Langmuir and Freundlich isotherms were used for the adsorption isotherm study. The non-linear forms of Langmuir and Freundlich isotherm models are shown in equations 3 and 4, respectively.

$$Q_e = Qm \frac{K_l \,.\, C_e}{(1 + K_l \,.\, C_e\,)} \tag{3}$$

$$Q_e = K_f . C_e^{\frac{1}{n}} \tag{4}$$

Where Q_m is the maximum adsorption capacity (mg/g), Q_e is the amount of adsorbate adsorbed per unit mass of adsorbent (mg/g), K_l is the Langmuir constant (L/mg), C_e is the equilibrium concentration of residual MB dye (mg/L), and K_f is the Freundlich constant (L/g) associated with the adsorption capacity and $\frac{1}{n}$ is the dimensionless heterogeneity factor.

4.2.7 Adsorption kinetics

The adsorption kinetics experiment was performed using the optimum condition of parameters produced by the RSM model. In several conical flasks, the predicted initial dye concentration with the pH dye solution was prepared and the optimum amount of adsorbent was added to these flasks and then mixed thoroughly to ensure uniform mixing. Periodically sample the solution from each flask for the next 250 min and measure the remaining dye concentration using analytical techniques such as UV-Vis spectroscopy. Plot the data of dye concentration versus time to analyze the adsorption kinetics.

4.2.8 Antibacterial activity of G-rGO

The antibacterial activity of G-rGO was investigated against *Staphylococcus aureus* and *E. coli.* In this study, a sterile nutrient agar medium was prepared and cast into the petri dish and left for some time at room temperature to solidify. Subsequently, a 10 μL well-developed *S. aureus* and *E. coli.* culture was evenly distributed over the Petri dish and placed in a laminar airflow for 10 min. Further, 5-8 μL of G-rGO solution with different concentrations of 20, 40, and 80 μg/mL were dropwise placed over the bacteria with 20 μg/mL solution of GO as a control on the Petri dish according to different marked places on the Petri dish. Antibacterial activity was examined after 12 h incubation duration (30±5°C). Further, the zone of inhibition was calculated by measuring the circular diameter of the *S. aureus* and *E. coli.* Culture-free area on the petri dish.

4.2.9 Optimization of adsorption using Response Surface Methodology (RSM)

RSM was used for optimization of the adsorption of MB dye by using a Central composite design (CCD) method. CCD was satisfactorily used to examine the impact of various factors on the effectiveness of MB dye's adsorption onto G-rGO. The ranges and levels of four independent variables were chosen: pH (A), G-rGO dose (B), initial dye concentration (C), and time (D) are mentioned in **Table 4.1**. The response of the system was defined by the percentage of MB dye removal. The optimal point prediction model based on a quadratic equation was expressed in Equation (5).

$$Y = \beta_0 + \sum_{i=1}^{k} \beta_i x_i \sum_{i=1}^{k} \beta_{ii} x_i^2 + \sum_{i=1} \sum_{j=1+1} \beta_{ij} x_i x_j + \varepsilon \qquad (5)$$

Where, Y: response (dependent variable), β_0 constant coefficient, β_i; β_{ii}; β_{ij}: coefficients for the linear, quadratic, and interaction effects,x_i; x_j: factors (independent variables) and ε: error. A standard RSM-based CCD was used to study the percentage removal of MB dye. Thirty experimental runs were carried out in triplicate by the specified scheme mentioned in **Table 4.2**. The data obtained was evaluated by graphical analysis and regression using Design Expert Version 13.0.5.0. The model's fitness and results were examined using analysis of variance (ANOVA). The optimum values of the four independent parameters were determined by analyzing the response surface contour plots and solving the regression equation. The coefficients of multiple determination (R^2) were used to explain the variability of the dependent variables, and the prediction of optimum value and how the factors interacted with one another within a specified range was demonstrated by using the model equation.

Table 4. 1 Independent process variable experimental range and levels.

Independent variables	Designated symbol	Levels and ranges (coded)				
		-α	-1	0	+1	+α
pH	A	2.5	5	7.5	10	12.5
Adsorbent dose (mg/100 mL)	B	5	20	35	50	65
Initial MB concentration (mg/L)	C	15	30	45	60	75
Time (min)	D	15	60	105	150	195

Table 4. 2 Central Composite Design experimental matrix.

Run	pH	Adsorbent dose	Initial concentration	Time	% Removal	
	A	B	C	D	Experimental	Predicted
1	7.5	5	45	105	79.67	78.64
2	7.5	65	45	105	94.87	94.42
3	7.5	35	75	105	88.51	87.39
4	7.5	35	45	105	90.89	89.93
5	7.5	35	45	105	88.32	89.93
6	5	50	60	60	85.15	87.45
7	7.5	35	15	105	67.47	67.11
8	12.5	35	45	105	64.92	65.29
9	10	20	60	150	75.15	75.49
10	10	20	60	60	69.63	70.42
11	5	20	30	150	50.15	51.41
12	10	50	30	60	89.85	89.76
13	10	50	30	150	95.9	96.44
14	5	20	30	60	41.25	41.84
15	7.5	35	45	105	90.58	89.93
16	5	50	30	60	61.2	60.48
17	5	20	60	150	90.33	92.28
18	7.5	35	45	15	72.54	73.15
19	5	50	30	150	67.35	68.43
20	10	20	30	60	73.91	73.88
21	5	20	60	60	86.86	85.93

22	10	50	60	150	71.35	72.63
23	10	20	30	150	82.6	82.17
24	10	50	60	60	70.83	69.18
25	2.5	35	45	105	54.65	52.80
26	5	50	60	150	92.53	92.18
27	7.5	35	45	105	89.82	89.93
28	7.5	35	45	195	88.27	86.18
29	7.5	35	45	105	90.07	89.93
30	7.5	35	45	105	89.92	89.93

4.3 Result and Discussions

4.3.1 Characterization of GO and G-rGO

4.3.1.1 HR-XRD of GO and G-rGO

Powder X-ray diffraction analysis was carried out to validate the formation of the crystalline nature of as-synthesized GO and the amorphous nature of G-rGO, and listed in **Fig. 4.2.** The Bragg's equation was used to determine the d-spacing values, which are described as $d = n\lambda/2 \sin\theta$, where d stands for d-spacing or interplanar spacing, $\lambda = 1.540$ Å (wavelength of X-rays transmitted), θ indicates peak position (in Radians), order of diffraction ($n = 1$). Graphite, in its purest form, at $2\theta = 26.63°$ had a sharp peck corresponding to layer structures that are well-organized along the orientation (002) [145]. Although Hummers' method involved interaction with $KMnO_4$ and H_2SO_4 (strong oxidants), this peak's intensity and sharpness were reduced severely [146]. Also, a new peak (001) at $2\theta = 11.77°$ corresponding to functional groups that contain oxygen appeared, having a 0.751 nm d-space value. Compared to G-rGO, the peak disappeared because of the reduction of GO by *T. cordifolia* stem extract. A less intense and broad reflection peak (002) was observed at $2\theta = 22.81°$ for G-rGO with a 0.389 nm d-space value. The greater value of d-space in GO indicated that O_2 functional groups are formed and water molecules intercalate between graphite layers. The decreased value of the d-spacing of G-rGO indicated that exfoliation had occurred more extensively because oxygen-related groups from the GO surface were removed [147]. The reduction of GO includes the reduction or elimination of oxygenated functional groups on GO, resulting in the restoration of the sp^2 carbon structure of graphene. The less intense and broader peak of G-rGO suggests a decrease in the crystallinity and long-range order compared to the highly ordered structure of GO. The broadening of the peak indicated the transformation of GO into a more disordered and defective structure, providing insights into the reduction process and the resulting properties of G-rGO. The G-rGO's XRD pattern mostly matched the previously reported graphene pattern [148].

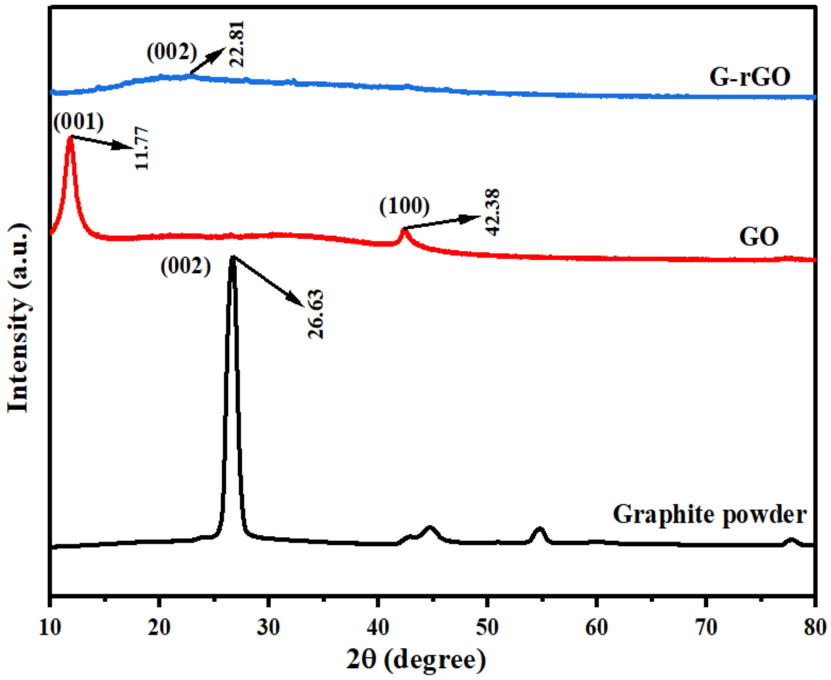

Fig. 4. 2 XRD spectra of Graphite powder, GO, and G-rGO.

4.3.1.2 FTIR analysis of GO and G-rGO

FTIR spectrum depicted the functional group transformation of GO before and after reduction and is presented in **Fig. 4.3**. The C=O stretching vibrations of carbonyl groups were shown strongly in the GO’s FTIR spectra at 1716 cm^{-1} [149]. O-H stretching vibrations and high loading of hydroxyl (-OH) group at 3,190 and 1220 cm^{-1}, C=C at 1,615 cm^{-1}, C=C bending 973

cm^{-1}, and 666 cm^{-1} found in GO's spectra. In G-rGO, the reduction in the intensity of the peak shows the elimination of groups [150,151]. The intensities of peaks associated with oxygen functions, such as the C=O stretching peak and the O-H deformation peak, were considerably decreased, implying that graphene oxide has reduced. FTIR analysis confirmed the effective synthesis of graphene oxide and the reduction of graphene oxide (GO). Further, the FTIR spectrum of *T. cordifoila* plant extract was also depicted in **Fig. 4.3.** The presence of -OH and -NH stretching is confirmed by the broad peak at 3334 cm^{-1}. This overlapped vibration was a result of the presence of amino groups and phenol/carboxylic groups of alkaloids in the extract of *T. cordifolia* [152,153]. Extremely faint peaks observed at 2125 cm^{-1} represent a $C\equiv C$ stretching of alkanes. A peak confirmed NH_2 scissoring and N-H bend of primary amines 1635 cm^{-1} [153]. The narrow peak at 654 cm^{-1} confirmed the presence of C-Br, and C-I stretching.

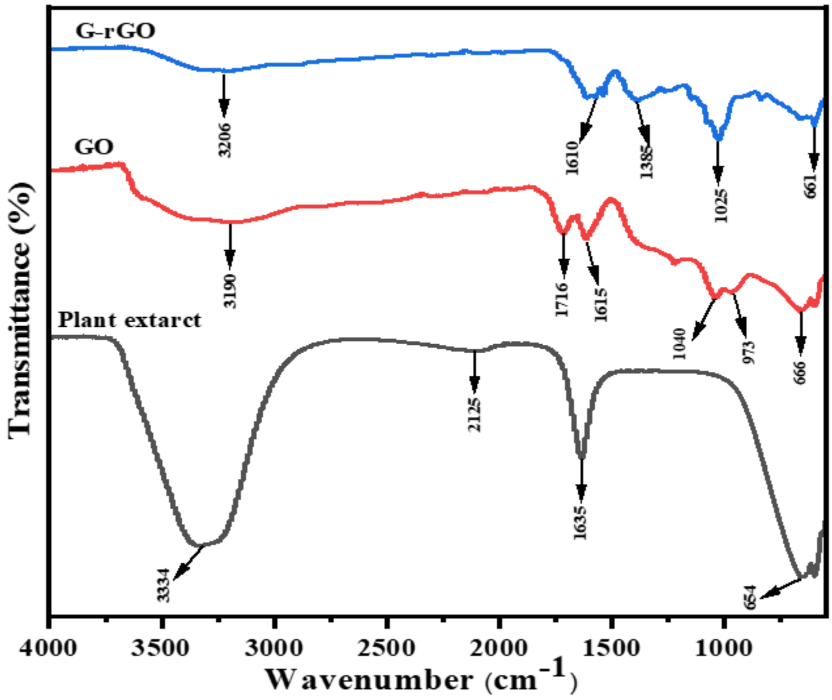

Fig. 4.3 FTIR spectral illustration of plant extract, GO, and G-rGO from *T. cordifolia* plant extract.

4.3.1.3 UV-Vis absorption spectra of G-rGO

The UV-Vis spectra of G-rGO show (**Fig. 4.4a**) that G-rGO has a maximum absorption peak at λ_{max}= 263 nm, indicating the removal of certain groups on the GO surface and the electronic conjugation has been restored after the reduction of GO [154,155]. This shift signifies heightened π-electron density and enhanced structural organization, aligning with the revival of sp^2 carbon and potential atomic reorganization [156].

The following Tauc's equation was used to determine the optical band gap energy of the G-rGO based on the UV-Vis findings.

$$(\alpha h\nu) = A\left(h\nu - E_g\right)^{n} \qquad (6)$$

where α abbreviates for absorption coefficient, h is Plank constant (6.626×10^{-34} J.s), *ν* represents the frequency of incident light, A is constant, E_g denotes optical energy band gap of the semiconductor TiO_2, and n is ½ for direct allowed transitions. The optical band gap energy was calculated from the extrapolation of the linear region to the x-axis of the $(\alpha h\nu)^2$ against the hν graph (**Fig. 4b**). It was found that G-rGO obtained a 2.43 eV optical energy band gap (E_g). A similar trend was reported for the reduction of the GO using lemon juice as a reducing agent and microwave-irradiated partially reduced GO [157,158].

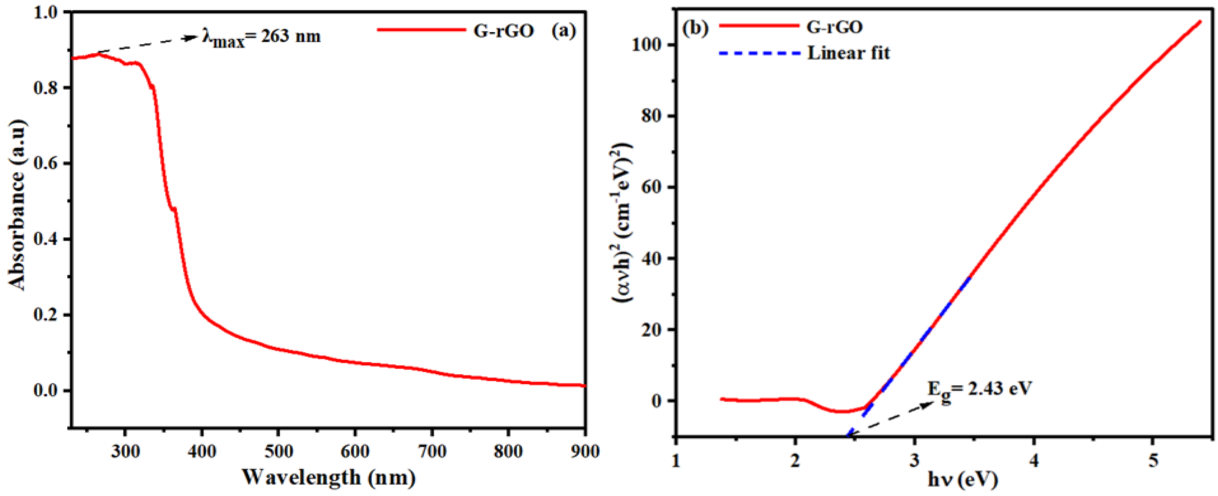

Fig. 4. 4 An illustration of (a) absorption spectra of G-rGO and (b) Tauc's plot for calculation of the energy band gap of G-rGO through linear extrapolation.

4.3.1.4 Zeta Potential and Hydrodynamic particle size of GO and G-rGO

G-rGO has a higher conductivity and is more soluble in water than GO. Zeta potential was used to evaluate the stability of the colloidal dispersion. For solvents in GO or G-rGO dispersed solution, the intensity of electrostatic repulsion between similarly charged vicinal sheet surfaces is indicated by the magnitude of the zeta potential. The average value of zeta potential was found to be -29.90 mV for G-rGO, which was higher than 11.50 for GO (ζ =-18.40 mV), demonstrating the increased stability of G-rGO colloidal dispersion **(Fig. 4.5a and b)** [159]. G-rGO, with fewer oxygen functional groups and more sp^2 carbon regions, was formed due to the reduction of GO. The increased sp^2 domains allowed for stronger π-π stacking interactions between G-rGO and facilitated the formation of a more compact and stable G-rGO structure. The hydrodynamic radius of G-rGO particles was less than that of GO [160]. The range of hydrodynamic radius of G-rGO was 270-470 nm, and for GO, it was 480-850 nm (**Fig. 4.5c).** The smaller size of a particle means a higher surface area of particles, which is favorable for adsorption [161].

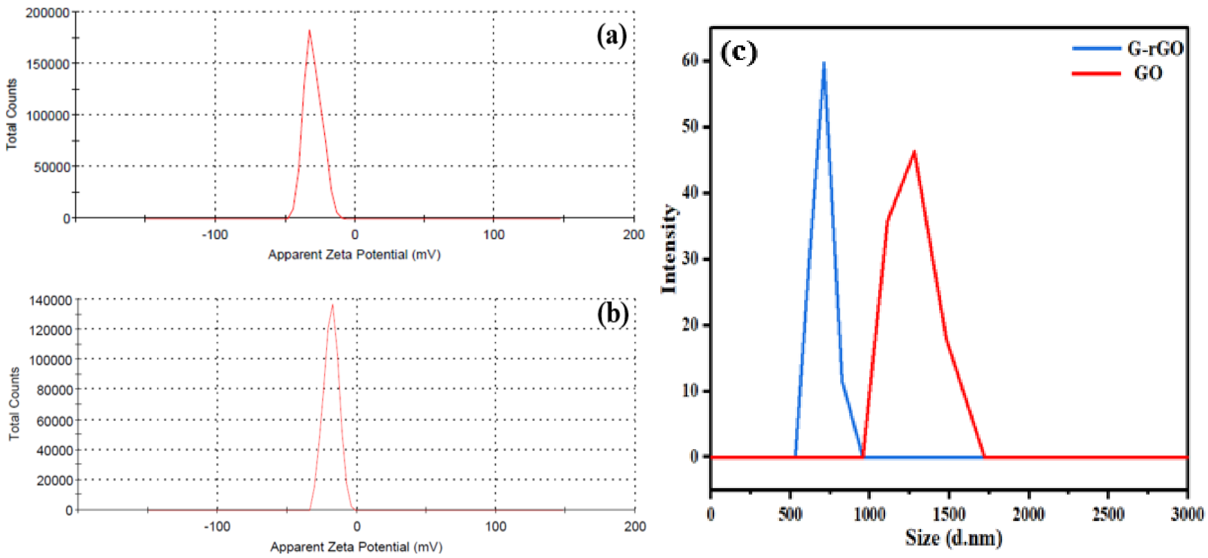

Fig. 4. 5 The Zeta Potential distribution according to total counts and intensity, (a) G-rGO (b) GO (c) A typical representation of the GO and G-rGO size distribution.

4.3.1.5 SEM and EDX analysis of GO and G-rGO

GO and G-rGO's SEM images are shown in **Fig 4.6a and b**. G-rGO microstructure showed folded and wrinkled sheets (**Fig 4.6b),** demonstrating that G-rGO was exploited effectively with less thickness. G-rGO samples had flaky, scale-like structures and resembled closely restacked, undulating silk waves. G-rGO consists of nanosheets with an average width of approximately 30 nm, and the range of the width of G-rGO nanosheets is 20-35 nm. They consisted of discrete, closely interconnected nanosheets, and the outcomes were aligned with resveratrol's reduction of GO [162]. The diminished interplanar distance was the result of the elimination of oxygenated groups from the edges and basal planes of G-rGO. This observation was consistent with the XRD results of GO and G-rGO, which showed that G-rGO has a shorter d-spacing than GO. EDX was used to analyze the elemental composition of GO and G-rGO **(Fig 4.6c and d)**. The EDX spectral analysis revealed the O atomic percentage present in G-rGO (19.90%) and GO (40.45%) (**Table 4.3**). Because oxygen-carrying functional groups had been removed from the surface of GO, the oxygen atomic % had decreased [163].

Table 4. 3 The EDX analysis of GO and G-rGO.

Element	GO (wt.%)	G-rGO (wt.%)
C	59.55	66.37
O	40.45	13.73
N	-	19.90

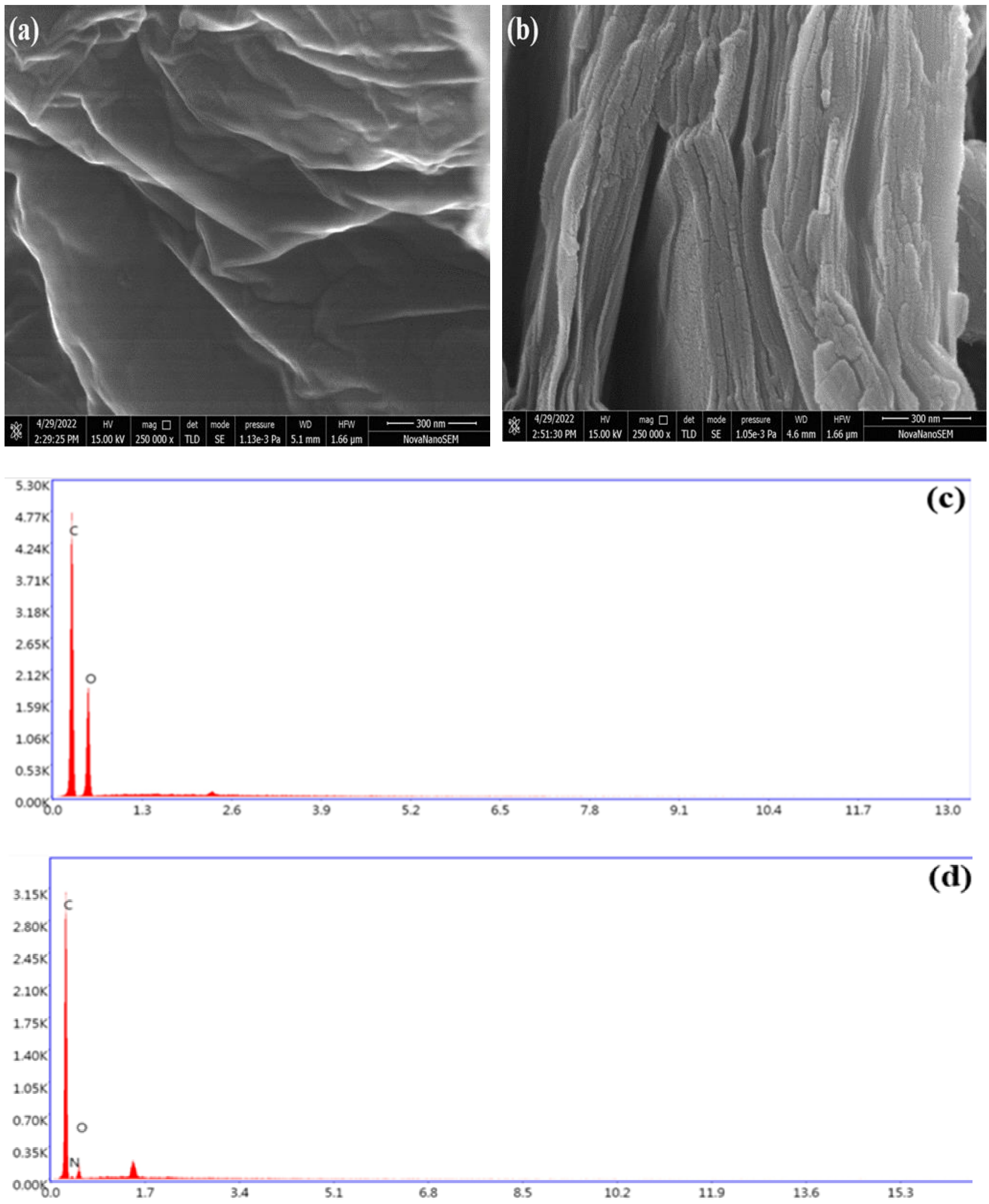

Fig. 4. 6 SEM micrographs of (a) GO and (b) G-rGO at ×250K times magnifications, EDX analysis of (c) GO and (d) G-rGO.

4.3.2 Estimation of removal of MB dye using Response Surface Methodology (RSM)

A batch study was conducted to examine the effect of various parameters on dye removal. As compared to other parameters, dye removal was found to be more influenced by pH, adsorbent dosage, initial concentration of dye, and time [164]. Therefore, these four parameters were chosen for the present study. A desorption study was additionally carried out, and it was discovered that employing an alkali solution resulted in a higher rate of dye desorption from the adsorbent. The outcomes of every experiment run by the software are shown in **Table 4.2.** The below-mentioned quadratic model describes an empirical relationship between the independent variables and the response.

$$\%\,removal = -\ 219.96227 + 34.98883 \times A + 1.5855 \times B + .77553 \times C + 0.434651 \times D - 0.018333 \times A \times B - 0.317033 \times A \times C - 0.002844 \times A \times D - 0.019028 \times B \times C - 0.000600 \times B \times D - 0.001194 \times C \times D - 1.23553 \times A^2 - 0.003781 \times B^2 - 0.014093 \times C^2 - 0.001268 \times D^2 \tag{6}$$

The findings of the ANOVA analysis confirmed that each parameter contributed to the favored result. The ANOVA statistics for the MB dye adsorption procedure are shown in **Table 4.4**. The proposed model's F-value was found to be 183.67, indicating that it was significant. The p-value must be less than 0.05, which is analogous to a significant model. In our model, this value was estimated to be less than <0.0001. The model would not be significant if any of the values A (<0.0001), B (<0.0001), C (<0.0001), D (<0.0001), A^2 (<0.0001), and D^2 (<0.0001) were larger than 0.1000; however, in this situation, all such values were less than 0.0001. The ANOVA displaying p-values higher than 0.05 ($p > 0.05$) for interactions AB, AD, and BD suggests that these specific interactions do not exert statistically significant effects on the adsorption process. This could be attributed to several factors: firstly, the combined effects of variables A and B (AB), A and D (AD), and B and D (BD) may be relatively weak or negligible, indicating that changes in one variable may not significantly impact adsorption behaviour when considered alongside changes in another variable. Secondly, the observed variability in the response variable, potentially due to experimental noise or uncontrolled factors, may overshadow any effects attributable to these interactions. Thirdly, the study's sample size and experimental design may lack the sensitivity to detect subtle interaction effects, especially if these effects are small or if the variability in the response variable is high. The values of the constants obtained from both coded and real data are displayed in **Table 4.4**. Additionally, the linear regression coefficients (R^2), which have a very high value of 0.9942 and indicate an excellent fit between the predicted and actual responses, also define the quality of regression. Moreover, The Predicted R^2 (0.9695) and the Adjusted R^2 (0.9888) were logically consistent (**Table 4.5**), demonstrating the model's ability to predict the process. The signal-to-noise ratio was evaluated using Adequate Precision. A numerical value >4 is preferred for modeling. In this study, it was evaluated to be 51.13, suggesting an adequate signal. This model can be applied to navigate the design space.

Table 4. 4 ANOVA analysis of the quadratic model (CCD) to estimate the % of MB dye removal.

Source	**Sum of Squares**	**Df**	**Mean Square**	**F-value**	**p-value**	
Model	5864.61	14	418.90	183.67	< 0.0001	Significant
A-pH	234.00	1	234.00	102.60	< 0.0001	
B-dose	373.51	1	373.51	163.77	< 0.0001	
C-initial concentration	617.12	1	617.12	270.59	< 0.0001	
D-time	254.41	1	254.41	111.55	< 0.0001	
AB	7.56	1	7.56	3.32	0.0886	
AC	2261.48	1	2261.48	991.59	< 0.0001	
AD	1.64	1	1.64	0.7184	0.4100	
BC	293.27	1	293.27	128.59	< 0.0001	
BD	2.62	1	2.62	1.15	0.3004	

CD	10.40	1	10.40	4.56	0.0496	
A^2	1635.58	1	1635.58	717.15	< 0.0001	
B^2	19.86	1	19.86	8.71	0.0099	
C^2	275.77	1	275.77	120.92	< 0.0001	
D^2	180.75	1	180.75	79.25	< 0.0001	
Residual	34.21	15	2.28			
Lack of Fit	30.24	10	3.02	3.81	0.0764	not significant
Pure Error	3.97	5	0.7936			
Cor Total	5898.82	29				

Table 4. 5 The correlation coefficient for the proposed model.

R^2	0.9942	C.V. %	1.92
Adjusted R^2	0.9888	Mean	78.48
Predicted R^2	0.9695	Std. Dev.	1.51
Adequate Precision	51.1293		

In this case, the coefficient of variance (CV %) predicted R^2 value was substantially closer. Therefore, it can be concluded that these values validated the model. In **Fig. 4.7a,** the relationship between the actual and predicted % removal was 1.92 %, demonstrating that the standard deviation was lower than the mean. The adjusted R^2 value and the MB dye were depicted. The actual experimental response values were substantially closer to the anticipated value of the % removal of MB. That conclusive indicated that the developed model accurately predicted the % removal of MB. **Fig. 4.7b** represents the standard plot of residuals, which shows the relationship between the internally studentized residuals and normal % probability. It can be concluded that the errors were distributed because residuals were generally scattered along a linear line. The internal studentized residuals and predicted values for the % of MB dye removal were correlated in **Fig. 4.47c.** The randomly distributed plot demonstrated that for all of the obtained responses, the variance of originally collected data remains the same [165]. Internally studentized residuals and run numbers for the % removal of MB dye were correlated and shown in **Fig. 4.7d.** This plot revealed that there was no valid correlation between experimental data points and the outcomes observed. The Design Expert software generated multiple runs for various independent variables. It was evident by examining every parameter that CCD passes every statistical test [166].

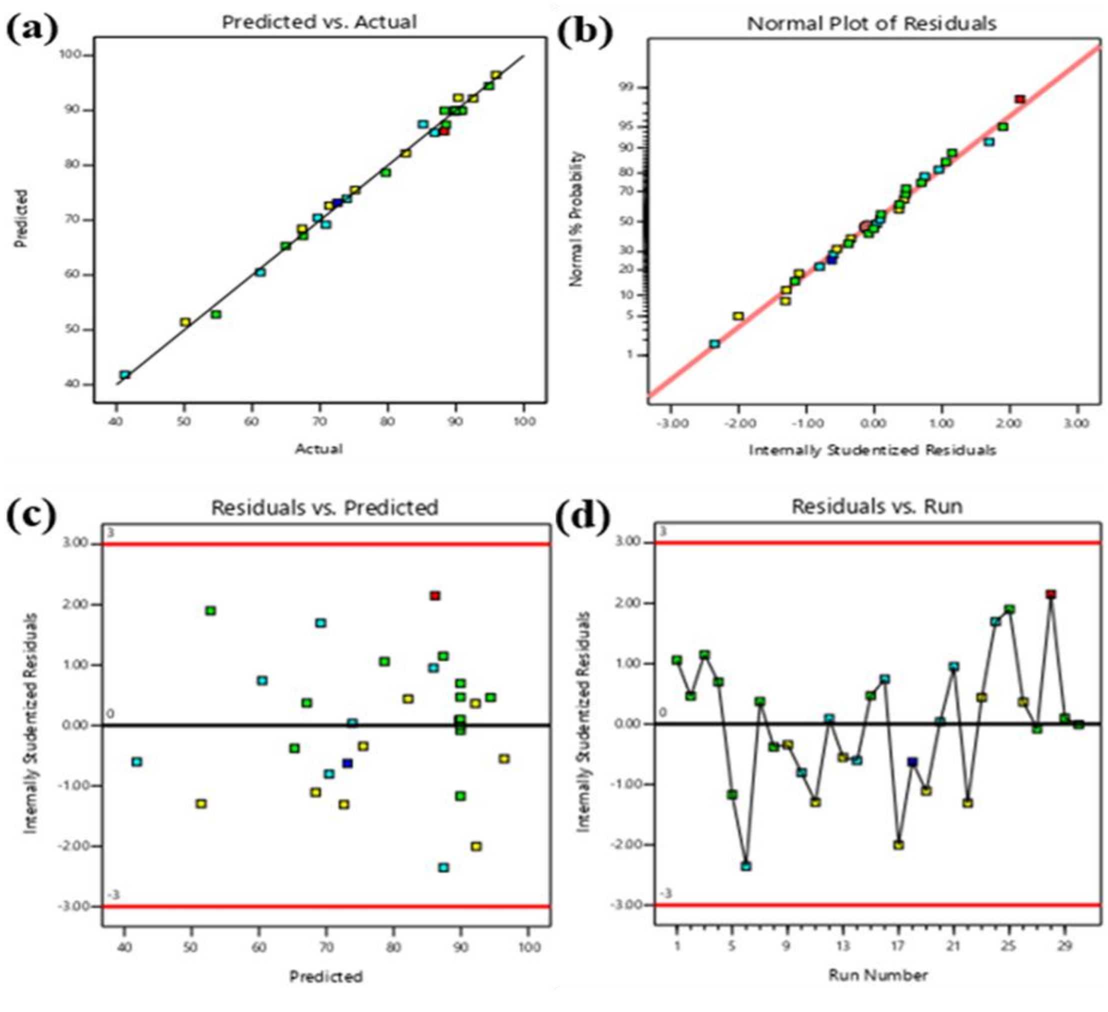

Fig. 4. 7 (a) The plot of actual vs predicted % removal of MB dye (b) The internally studentized residuals against the normal % probability plot of the % removal of MB dye (c) The graph between internally studentized residuals and the predicted % removal of MB dye (d) The graph between Internally studentized residuals and the run number.

4.3.2.1 Analysis of contour graphs and 3-D surfaces

The selected model for the study was generally represented by 3-D curves and contour plots. It provided a precise depiction of the response of the final output in the preferred domain of analysis and the performance of independent variables. The 3-D surface and contour plots demonstrated in **Fig. 4.8a and b**, respectively, correlated pH (A) and adsorbent dose (B) with the final response of % removal of MB dye. According to these figures (**Fig. 4.8a and b**), at low pH and a high adsorbent dose, the % removal of MB would have the maximum possible value. The interaction between pH (A), initial MB dye concentration (C), and % MB dye removal was illustrated by the 3-D surface and contour plot shown in **Fig. 4.8 (c) and (d).** The contour plot and 3-D curve revealed that the % removal of MB dye was highest at low pH and low initial MB dye concentrations. **Fig. 4.8e and f** depicted the relationship between pH (A), time (D), and % removal of MB dye. These figures showed that the amount of MB dye removed was greatest at high pH and long duration. Since the functional groups (-OH groups) on the surface of G-rGO deprotonated at high pH, they became more negatively charged, which improved the electrostatic interaction of the MB dye (positively charged) molecules with the G-rGO surface. Longer contact periods also resulted in greater binding between the G-rGO surface and MB molecules due to the chemosorption and stacking interactions that were created between the surface and the MB molecules. Longer contact time allowed MB dye molecules to permeate deeper into G-rGO's porous surface [167].

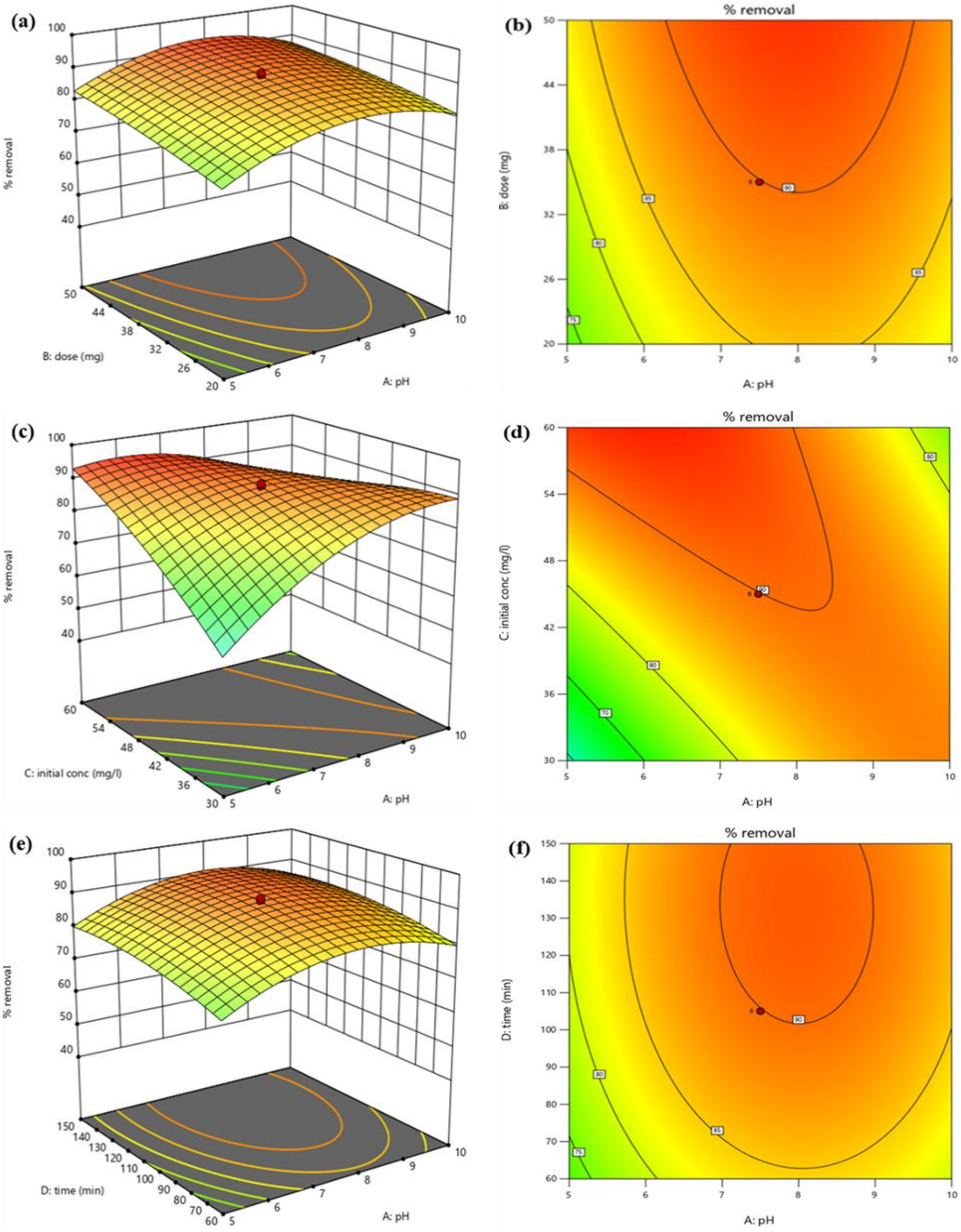

Fig. 4. 8 (a) 3-D surface illustration of pH (A), Adsorbent dose (B), and % Removal of MB dye (b) Contour plot demonstrating the effect of pH (A) and Adsorbent dose (B) on % Removal of MB dye (c) 3-Dimension response surface representation of pH (A), initial MB dye concentration (C), and % Removal of MB dye (d) A demonstration using Contour plot between the pH effect (A) and initial concentration of MB dye (C) on % Removal of MB dye (e) 3-D surface illustration of pH (A), time (D), and % Removal of MB dye (f) The effect of pH (A) and time (D) on % Removal of MB shown by contour plot.

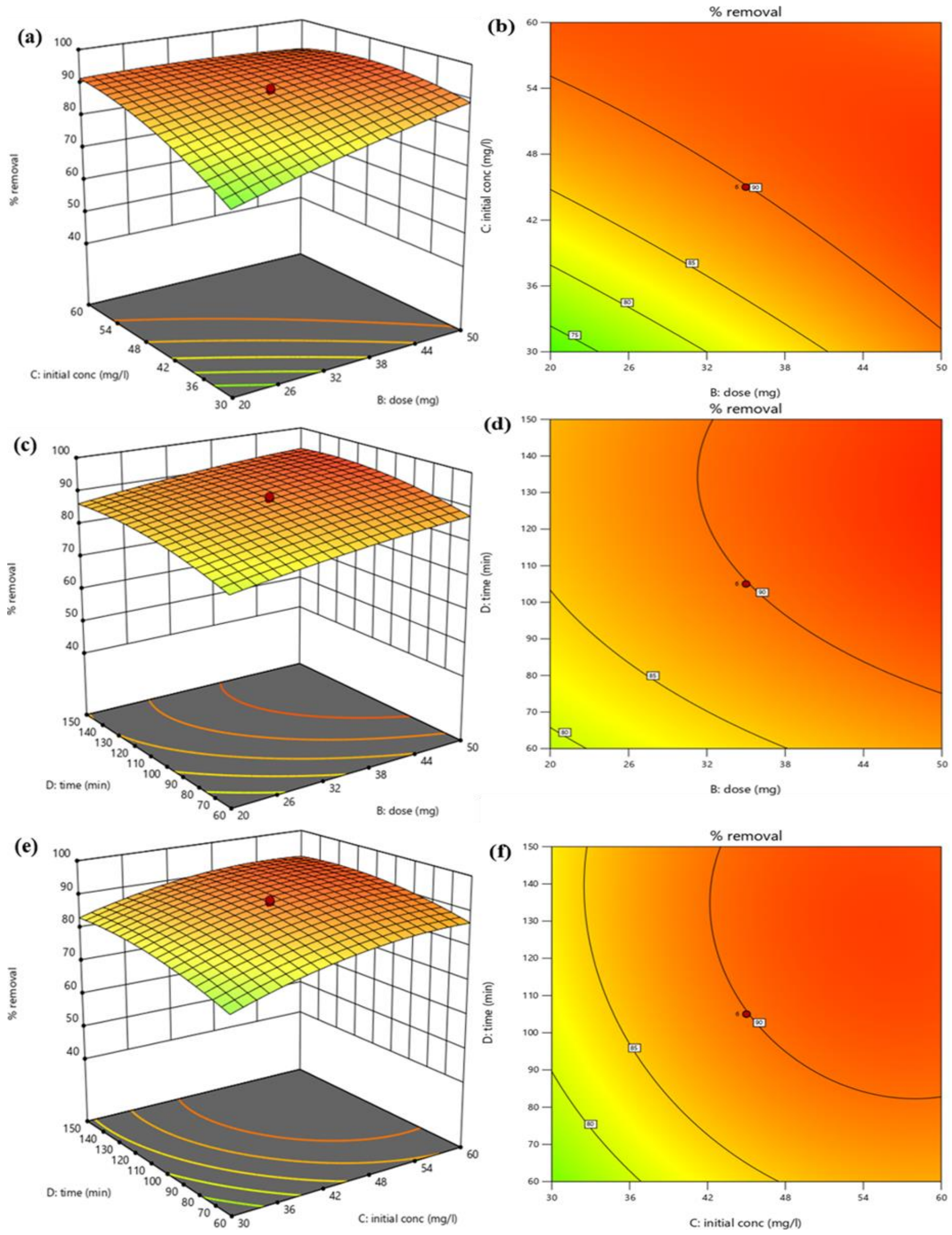

Fig. 4. 9 (a) 3-D surface illustration of Adsorbent dose (B), initial concentration of MB dye (C), and % removal of MB dye, (b) Contour plot demonstrating the Adsorbent dose effect (B) and initial concentration of MB on % removal of MB, (c) 3-D surface representation of Adsorbent dose (B), time (D), and % Removal of MB dye. (d) Contour plot demonstrating the Adsorbent dose effect (B) and time (D) on % removal of MB dye, (e) 3-D surface illustration of the initial concentration of MB (C), time (D), and % Removal of MB dye, (f) Contour plot showing the effect of initial concentration of MB (C) and time (D) on % removal of MB dye.

The 3-dimensional surface and the contour plot were demonstrated in **Fig. 4.9a and b,** respectively, which correlated adsorbent dose (B) and initial concentration of MB (C) with the % removal of MB dye. These plots proposed that at a high adsorbent dose and low pH, the value of the % removal of MB dye would be maximum. The 3-dimensional response surface and the contour curve depicted the relationship between the adsorbent dose, time (D), and % removal of MB dye in **Fig. 4.9c and d**. These plots concluded that the % removal of MB dye was highest at low pH and low initial MB dye concentrations. **Fig. 4.9e and f** depicted how the initial concentration of MB (C), time (D), and MB dye’s % removal interacted. Both plots concluded that the % removal of MB was highest at higher pH and time.

4.3.2.2 Optimization based on the desirability function

The desired outcomes for response and each variable have been elected in numerical optimization from design software. The potential objectives for response were to maximize, target within range, minimize, none, and specify an exact value for factors. For every mentioned parameter, the levels must be defined (minimum or maximum). Each objective can be given a weight to modify the specific desirability function's shape. A total desirability function was created by combining the objectives. The desirability function has a range of zero to one, zero for outside limits, and one for the goal. The attempt to achieve the goals initiates at an arbitrary point and proceeds until it reaches its peak. Due to the curvature in response surfaces, multiple maxima may exist, and how they interact with the desirability function. Finding the 'best' local maximum seems to have a greater tendency when starting from plenty of points in the design space. A multiple-response method was used to optimize any combination of objectives, including the initial MB concentration and pH of the solution, adsorbent dose, the time needed, and % of MB removal. Through numerical optimization, optimum points were used to generate ramp desirability (**Fig. 4.10**). The optimum local maximum was discovered by observing the response surface changes from the starting points to be at adsorbent dose 49.32 mg, initial concentration 30.58 mg/L, initial solution pH 9.52, and time 147.82 min, and MB dye removal of 96.13%. The temperature and agitation speed were 30±5°C, and 130 rpm, respectively. The obtained desirability value demonstrated that the anticipated function might adequately represent the desired conditions and experimental model.

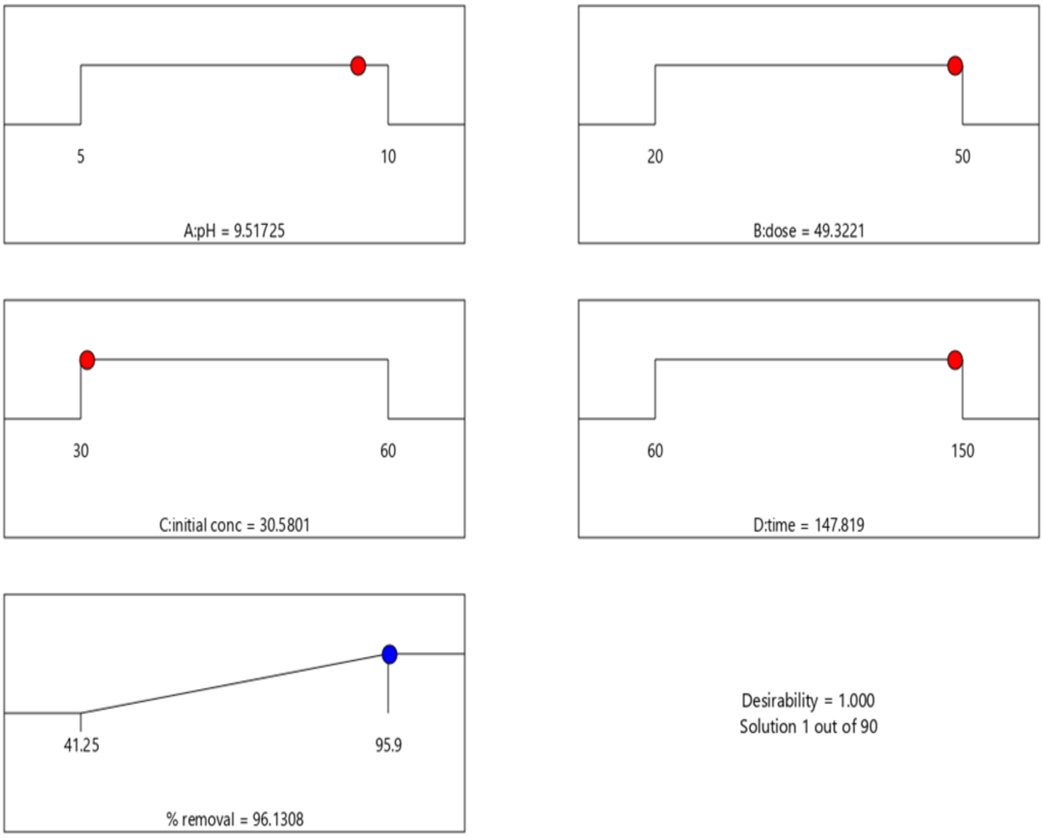

Fig. 4. 10 Desirability ramp for numerical optimization of objectives: initial pH of the solution, adsorbent dose, initial concentration of dye, time, and % removal of MB dye.

4.3.2.3 Confirmation experiments

Experiments were performed to validate the parameters predicted by the model (pH 9.52, initial MB concentration 30.58 mg/L, time 148 min, adsorbent dose 49.32 mg, agitation speed 130 rpm, and temperature 30±5°C) to support the predicted data generated through numerical modeling at optimized conditions. MB dye molecules in solution adsorb on G-rGO sheets through π-π stacking and electrostatic interactions. The surface area and conductivity of G-rGO enhance the breakdown of adsorbed molecules. Electron transfer from G-rGO reduces MB and converts it into less harmful compounds. G-rGO generates ROS, which aids in degradation through oxidative processes (**Fig. 4.11**). The MB dye removal was found to be 94.85% with a deviation of 1.29% and it was found below the permissible limit of the concentration of MB dye in textile effluent as per the Indian government guidelines [118,168]. It has been observed that there was a relatively minor deviation between the predicted % removal and actual % removal. Effective experimental design, validation of models, and a comprehensive understanding of the system's complexities are needed to enhance the accuracy of RSM predictions. The adsorption capacity at the corresponding optimum condition was found to be 58.81 mg/g.

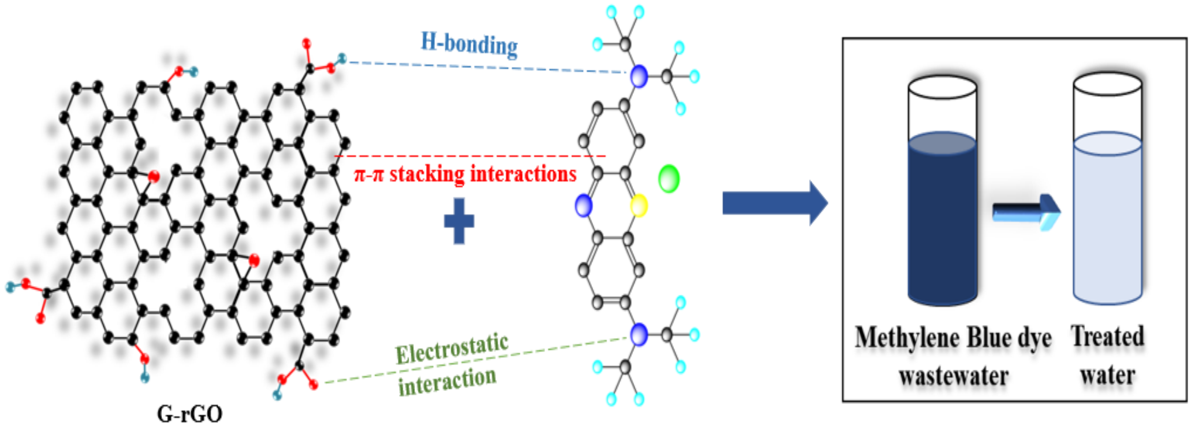

Fig. 4. 11 A schematic representation of the adsorption mechanism of MB dye degradation by G-rGO.

4.3.3 Adsorption isotherm

The suitable isotherm model shows adsorption capacity and how adsorption molecules have interacted between adsorbent and adsorbate at an equilibrium state in adsorption. Langmuir and Freundlich isotherm models are the most commonly used isotherm to represent the experimental data of adsorption. Both isotherms were used to study the adsorption of MB with

G-rGO (**Fig. 4.12).** The adsorption capacity exhibited an increasing trend, eventually reaching a plateau at its maximum. To determine the type of isotherm, the value of 1/n can be used in the Freundlich isotherm. The isotherm will be irreversible (1/n=0), undesirable (1/n>1), and desirable (0>1/n<1), and at n=1, adsorption linearly decreases. In this study, the 1/n value of Freundlich isotherm was 0.53, which shows an ideal adsorption performance [169]. Langmuir model showed better fitting with experimental findings (R^2 = 0.9928), which implies that MB dye adsorption on G-rGO occurred as a monolayer and at homogeneous sites [170]. The parameters of models were calculated for both the isotherms and shown in **Table 4.6**.

Table 4. 6 Langmuir and Freundlich isotherm model parameters.

S.N.	Langmuir Isotherm parameters	Freundlich Isotherm parameters
1.	Q_m = 160.45 mg/g	K_f = 7.92 L/g
2.	$K_l = 0.004$ L/g	n = 1.87
3.	R^2 = 0.9928	R^2 = 0.9650

According to the above finding, the G-rGO had a homogeneous surface and the MB dye was evenly entrapped in the surface.

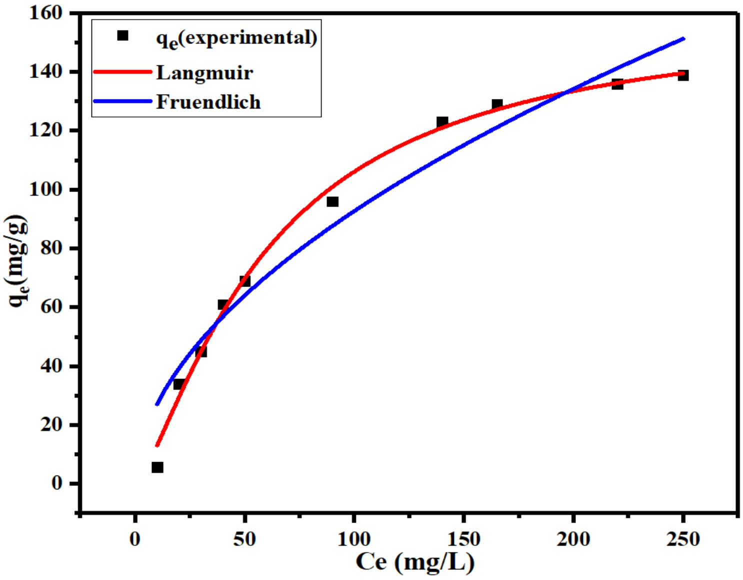

Fig. 4. 12 Evaluation of the stability of Freundlich and Langmuir isotherm models to explain the MB dye adsorption onto G-rGO.

4.3.4 Kinetic study

The adsorption kinetics was conducted concerning time. The UV-visible spectrophotometer was used to measure the absorbance of fractions of samples taken out at regular intervals as the reaction proceeded. The pseudo-first-order kinetic model assumes that the rate of adsorption is directly proportional to the number of available adsorption sites on the adsorbent surface, which is often the case for G-rGO materials with high surface area and abundant π-electron systems. The kinetic plot between $\ln \frac{C_0}{C_t}$ vs time was used to calculate the reaction's rate constant (**Fig. 4.13**). It was found that the adsorption process of MB dye on G-rGO was typically rapid initially, with a large number of dye molecules rapidly adsorbed onto the surface of the graphene. This initial rapid adsorption phase aligns well with the assumptions of the pseudo-first-order kinetic model. It was also found that the pseudo-first-order possesses the R^2 value 0.99343, which means the pseudo-first-order model closely predicts the adsorption behavior of MB on G-rGO.

$$\ln \frac{C_0}{C_t} = \mathrm{kt} \tag{7}$$

In this equation, C_0 and C_t are the MB dye concentration at the initial and final conditions, and k is the reaction's rate constant.

The reaction rate constant of adsorption of MB dye on G-rGO was determined from the slope of the graph between $\ln \frac{C_0}{C_t}$ vs time, and it was found to be $k = 0.00122\ \text{min}^{-1}$.

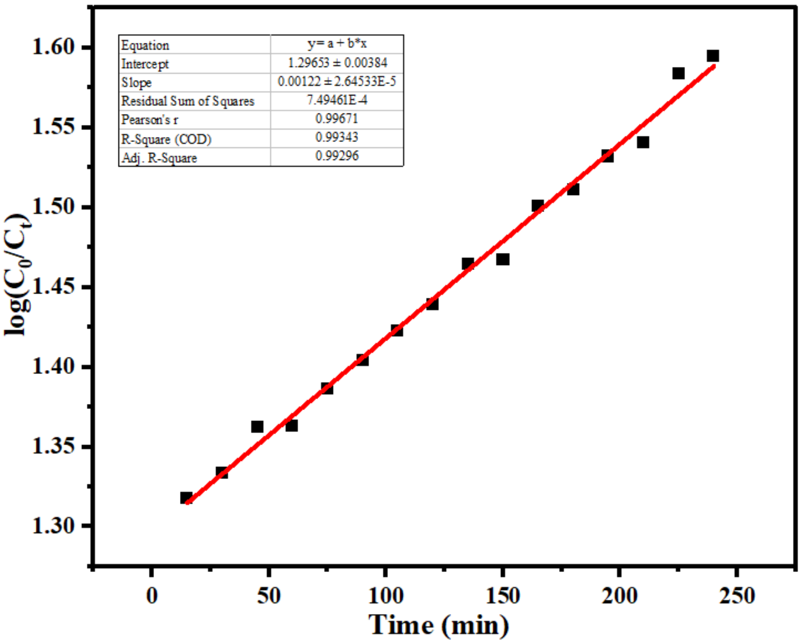

Fig. 4. 13 Kinetics of adsorption of MB on G-rGO, a linear fitted graph between $\ln \frac{C_0}{C_t}$ and time.

4.3.5 Recycling test of the adsorbent

Recycling the adsorbent after adsorption is an important and cost-effective procedure in wastewater treatment. The adsorbent must have high adsorption as well as good desorption capabilities to reduce the cost of adsorption significantly. Therefore, the regeneration and reuse of G-rGO were examined by separating G-rGO after the adsorption of MB dye (at optimum condition for 60 min adsorption duration) using centrifugation (300 rpm). The centrifuged adsorbent was added to the ethanol solution and stirred for 15 min. Then, it was filtered (Whatman 41 filter) rinsed with double distilled water several times, and then dried at 70°C. The same procedure was conducted four times to prove the efficient recovery and reuse of G-rGO [171]. It was found (**Fig. 4.14**) that a 14.74% decrement was observed in the % removal of MB dye after fresh to fourth recycle of G-rGO (85.52-72.89 %).

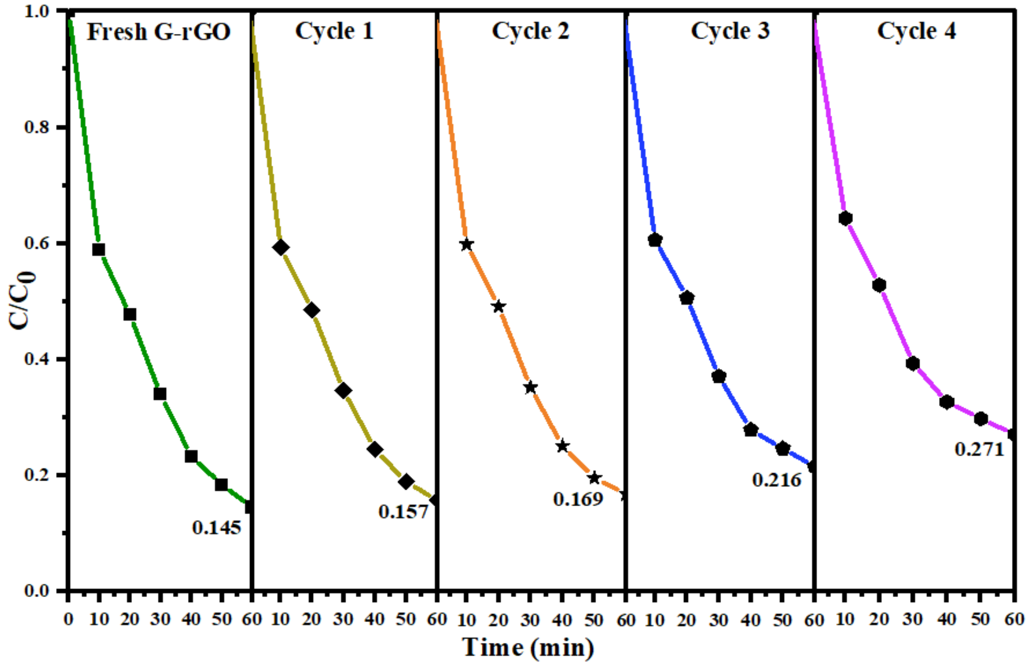

Fig. 4. 14 Recycling test of MB dye by G-rGO (initial MB concentration: 30 mg L^{-1}, adsorbent dose: 50 mg, pH: 9, agitation speed: 130 rpm, and temperature: 30±5°C)

4.3.6. Antibacterial activity of G-rGO

Escherichia coli (gram-negative) bacteria and *Staphylococcus aureus* (gram-positive) bacteria were used to investigate the antibacterial activity of G-rGO. *E. coli* and *S. aureus* have a spherical shape and smaller size. The growth of *S. aureus* and *E. coli.* were diminished at different marked places on the petri dishes having different amounts of G-rGO. It was observed that at 20, 40, and 80 µg/mL concentrations of the G-rGO with 20 µg/mL of GO as control incubated petri dish at 30±5ºC for 12 h, the zone of inhibition was measured approximately 10, 13, and 17 mm, and for control 8 mm, respectively (**Fig. 4.15a**) against *E. coli* gram-negative bacteria. Similarly, against *S. aureus*, the zone of inhibition was measured at approximately 10, 11, and 15 mm, and for control 9 mm, respectively (**Fig. 4.15b**). The primary mechanism by which G-rGO destructs bacteria cells is by mechanically stressing the cell membrane [151].

Reduction of GO to rGO restores the sp^2 carbon network and reduces the number of oxygen-containing functional groups, resulting in a more hydrophobic and biocompatible surface. This alteration in surface chemistry promotes stronger interactions between rGO and bacterial cell membranes, facilitating membrane disruption and increased penetration of rGO into bacterial cells. Additionally, the improved electrical conductivity of rGO enables efficient electron transfer processes, leading to oxidative stress and damage to bacterial DNA and proteins. Furthermore, the larger surface area and enhanced π-π stacking interactions of rGO enhance its ability to adsorb and immobilize bacterial cells, further contributing to its antibacterial efficacy (**Fig. 4.15c**). It shows the antibacterial property of G-rGO against gram-negative (*E. coli*) bacteria [172] as well as against gram-positive (*S. aureus*) bacteria [173].

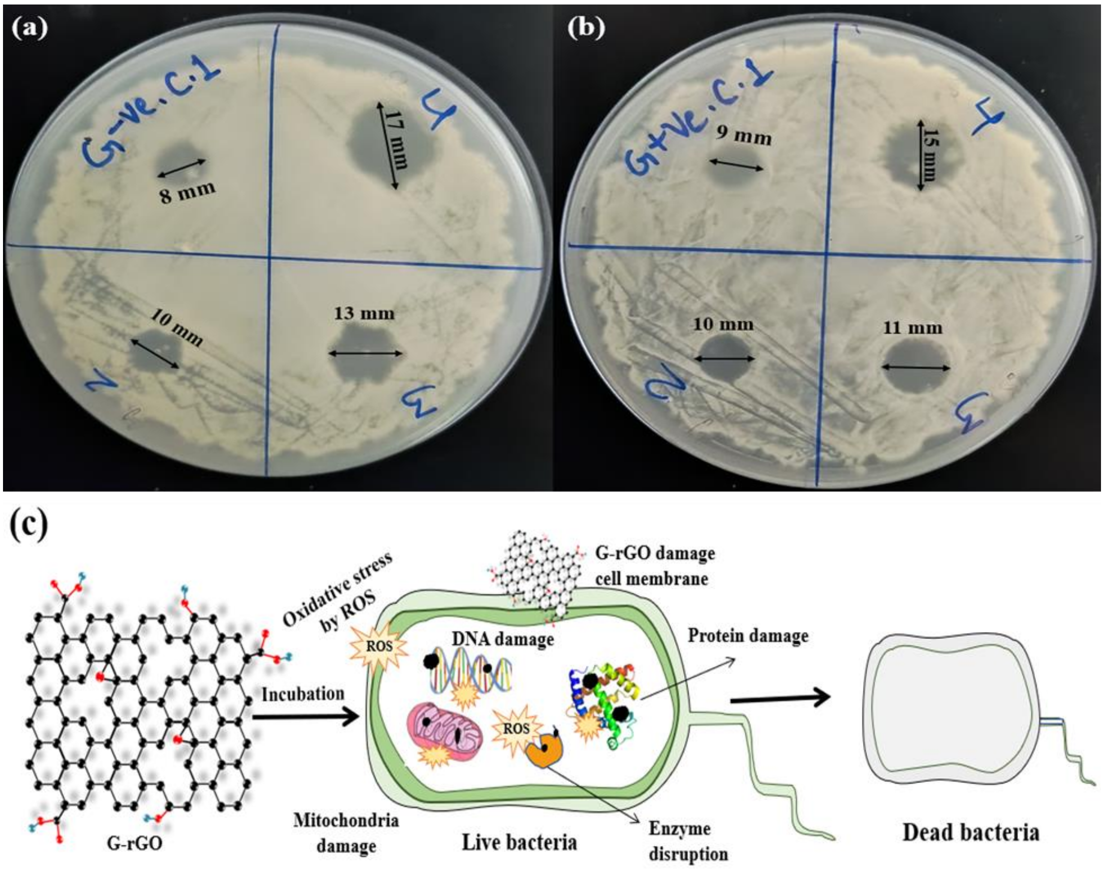

Fig. 4. 15 Petri dish shows the antibacterial potential of G-rGO against (a) *E. coli* (gram-negative) Bacteria, (b) *Staphylococcus aureus* (gram-positive) Bacteria, and (c) A schematic representation of the mechanism for antibacterial activity of G-rGO against bacteria.

4.4. Conclusions

The present work emphasizes the first-ever green production of G-rGO using naturally available *T. cordifolia* plant extract by reduction of GO. Modified Hummer's method was used to synthesize GO. The feed and extract were characterized using different analytical tools. Also, RSM is used to examine the combined impact of several process parameters on MB dye removal. The HD-XRD results confirmed an increased crystallinity of G-rGO, and FTIR confirmed an improved function group. The adsorption study of MB confirmed that under optimum conditions, the removal efficiency of the MB was determined to be 94.85%, with an adsorption capacity of 58.81 mg/g. The kinetics of adsorption linearly followed pseudo-first-order and obtained a 0.00122 min^{-1} rate constant of the reaction. Finally, the typical antibacterial activity was studied, and the findings supported the G-rGO's antibacterial activity against *S. aureus* and *E. coli*. Therefore, the present study finding exhibited green synthesis as an innovative, economical, and environmentally friendly approach for the formation of G-rGO and its excellent antibacterial activity.